INTERNATIONAL JOURNAL OF HYDROGEN ENERGY 45 (2020) 25541–25554

Available online at www.sciencedirect.com

ScienceDirect

journal homepage: www.elsevier.com/locate/he

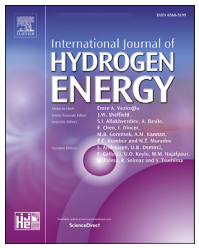

Fracture strain model for hydrogen embrittlement based on hydrogen enhanced localized plasticity mechanism

Song Huang, Yalin Zhang, Chao Yang, Hui Hu *

School of Mechanical and Power Engineering, East China University of Science and Technology, Shanghai, 200237, PR China

HIGHLIGHTS

- Continuum damage model for hydrogen embrittlement based on micro-void coalescence.
- Description of hydrogen-assisted void growth and coalescence with HELP mechanism.
- Practical model cover ductile and brittle fracture with few model parameters.

ARTICLE INFO

Article history:
Received 9 January 2020
Received in revised form
7 June 2020
Accepted 26 June 2020
Available online 18 July 2020

Keywords:
Hydrogen embrittlement
HELP
Fracture strain model
Void growth and coalescence
Continuum damage model

ABSTRACT

Hydrogen energy is a candidate of the "ultimate energy". However, the quantified evaluation of hydrogen embrittlement phenomenon remains to be a challenging topic. This paper provides a continuum damage model to quantify hydrogen embrittlement. Firstly, theoretical model of the proposed method was introduced. The proposed model applied multi-axial fracture strain based ductile damage evolution law coupled with HELP mechanism to evaluate hydrogen accelerated micro-void coalescence (MVC) fracture. Void growth and coalescence were described by hydrogen enhanced plastic strain and hydrogen reduced fracture strain. Then, the proposed method was implemented on commercial finite element software package. Compact tensile (CT) test and slow strain rate tensile (SSRT) test of two commercial steels were investigated numerically and compared with available experimental results to verify the rationality of the proposed model. The results indicated the proposed method reproduced CT and SSRT tests result with different hydrogen concentrations precisely. Hydrogen's effect on MVC process was discussed. It is suggested HELP based MVC could be a viable model to quantify hydrogen embrittlement. The proposed method was also highlighted with the advantage of describing hydrogen's effect with only one parameter.

* *Corresponding author.*
E-mail address: huihu@ecust.edu.cn (H. Hu).

https://doi.org/10.1016/j.ijhydene.2020.06.271

Introduction

Hydrogen energy has been identified as a promising candidate of renewable energy source. Although with good characteristics of unlimited supply, zero carbon emission and high energy efficiency [1], hydrogen, especially pressurized gaseous hydrogen also plagues its containers with material damage phenomenon known as Hydrogen Embrittlement (HE). HE must be addressed to utilize hydrogen energy safely. The interpretation, description and prediction of HE is still a challenging and attractive topic.

There are two typical HE failure modes: Under low stress level, hydrogen assists subcritical growth of micro-crack, leading to unstable growth of crack when microcrack becomes critical, also known as hydrogen assisted cracking. Under high stress level, hydrogen enhancing fracture process accompany with micro-void coalescence (MVC) or matrix debonding, typically known as hydrogen reduced ductility [2,3]. Among all existing models interpreting HE, two mechanisms namely hydrogen enhanced decohesion (HEDE) and hydrogen enhanced localized plasticity (HELP) are most acceptable as they represents the most essential characters of HE. HEDE is based on the assumption that hydrogen lowers cohesive strength between metal atoms [4–6]. This mechanism is supported by extensive experimental observations of enhanced crack initiation ahead matrix discontinuities in hydrogen charge condition, which can be rationalized by hydrogen reduced atomic bonding strength [7–9]. HEDE is viable, especially for those stress controlled brittle fracture process. HELP mechanism states hydrogen reduces the resistance of dislocation motions which leads to enhanced localized dislocation activity that promotes fracture [10,11]. Extensive experiment evidences of HELP have been reviewed by Robertson et al. [12], Dadfarnia et al. [13], Martin et al. [14] and Milos et al. [15], indicating HELP is, at least a part of HE's essential. Furthermore, some investigations indicated that single HE mechanism may be insufficient to trigger macroscopic embrittlement [14,16]. Reasonable interpretations are known as HELP-meditated HEDE mechanism [17] and HELP + HEDE mechanism [18,19]. These mechanisms assume prerequisite of HELP during local deformation following synergistic or competitive effect of brittle and ductile fracture mechanisms depending on sophisticated material microstructure, loading and environment conditions [15]. In summary, although underlying mechanism of HE is still debatable [3,12], it is widely accepted that hydrogen enhanced plasticity plays an important role in most hydrogen-related fracture events. Besides, a brittle fracture based mechanism such as HEDE has its intrinsic deficiency as it cannot cover the ductile fracture dominated by MVC in hydrogen-free or unsusceptible cases [20]. Therefore, intensive quantifying investigation of HELP based HE model is inevitable and meaningful.

Modeling of hydrogen induced plasticity was proposed by Sofronis et al. [21] with a local softened flow stress depending on hydrogen concentration. Following this idea, Liang et al. [22–24] investigated hydrogen's effect on local plastic instability and MVC process. They found that coalescence of micro-voids is promoted by hydrogen through HELP mechanism. Ahn et al. [25] investigated the response of mesoscopic representative volume element (RVE) under the action of HELP. They further combined the response of RVE with a cohesive zone model (CZM) [26] to simulate ductile crack propagation behavior in the present of hydrogen. Brocks et al. [27] modeled hydrogen-induced cracking with HELP-meditated HEDE mechanism, where both hydrogen induced flow strength softening and hydrogen reduced cohesive strength were considered to reproduce cracking resistance curve of hydrogen-charged Compact tensile (CT) test. In the past decade, extensive published works performed CZM for hydrogen related crack simulation [28,29]. Both HELP and HEDE have been used to construct hydrogen dependent traction-separation laws (TSL) [26,30–34] for CZM. CZM based HE model is effective in reproducing laboratorial fracture mechanics test results. But CZM also requires elaborate preparation of crack path for applying cohesive element, which restricts its application in other hydrogen systems [28]. Continuum damage mechanics (CDM) based model offers an alternative HE modeling framework which avoids crack path pre-assign as CZM always does. In contrast to the popular CZM + HEDE method, the development of CDM based HE model is insufficient. Based on experimental observations, Kim et al. [35] attempted to describe HE with a stress-modified fracture strain model where fracture strain is linearly decreased with lattice hydrogen concentration. Jeon et al. [36] further developed this technique by combining material softening induced by HELP mechanism. Recently, hydrogen informed Gurson damage models was proposed by Yu et al. [20], where an additional parameter describing hydrogen enhanced void growth was introduced. HGurson model has been used to evaluate HE of advanced dual-phase steel [29]. However, noticeable problems of these CDM based HE model are: (1) How to rationalize the introduced parameter with acceptable HE mechanism, for example, with HELP. (2) How to reduce model parameters to keep it accurate as well as practical.

Following the work of Kim et al. [35] and Jeon et al. [36], the purpose of present work is to quantify HE with fracture strain based continuum damage model. An attempt was made to describe hydrogen-meditated MVC with just one model parameter. A numerical method with two-scaled mechanical responses was established. HELP mechanism was introduced to capture hydrogen's effect on damage evolution. The performance of the proposed method was then verified by existing Compact Tensile (CT) test and Slow Strain Rate Tensile (SSRT) test results of commercial steels.

Theoretical model

Hydrogen concentration in equilibrate state

Hydrogen atoms in metal is assumed to be located in Normal Interstitial Lattice Sites (NILS) and in dislocation hydrogen

trap sites. In the present work, equilibrium hydrogen distribution described by Sofronis et al. [21] is applied. Hydrogen diffusion in NILS obeys Fick's law, which is driven by hydrostatic stress. Under quasi-static loading condition, NILS hydrogen can be assumed to be in equilibrium state. The occupancy of NILS hydrogen is

$$\frac{\theta_L}{1-\theta_L}=\frac{\theta_L^0}{1-\theta_L^0}K_L \tag{1}$$

where θ_L is the NILS hydrogen occupancy. Subscript "0" denotes the stress free state. Equilibrium constant K_L is

$$K_L=\exp\left(\frac{\sigma_m V_H}{RT}\right) \tag{2}$$

where σ_m denotes mean stress. V_H is partial molar volume of hydrogen. R is constant of ideal gas. T is temperature in Kelvin. The relationship between hydrogen occupancy and hydrogen concentration (H atom/m^3) is given as

$$C_L=\beta\theta_L N_L \tag{3}$$

where β is the number of NILS hydrogen site per host metal atom. N_L is the number of metal atoms in a unit volume. It can be calculated with

$$N_L=\frac{N_A}{V_M} \tag{4}$$

where N_A is Avogadro's constant. V_M is molar volume of host metal.

The equilibrium between trapped hydrogen and NILS hydrogen can be described with Oriani's theory [37] as

$$\frac{\theta_T}{1-\theta_T}=\frac{\theta_L}{1-\theta_L}K_T \tag{5}$$

where θ_T is the trapped hydrogen occupancy. K_T is the equilibrium constant depends on the binding energy W_B of hydrogen trap, which is

$$K_T=\exp\left(\frac{W_B}{RT}\right) \tag{6}$$

Similar to Eq. (3), hydrogen concentration (H atom/m^3) in trap site can be stated as

$$C_T=\alpha\theta_T N_T \tag{7}$$

where α is the number of hydrogen site per trap. N_T is the density of hydrogen trap. N_T is stated as

$$N_T=\Lambda\frac{\rho}{a} \tag{8}$$

with [38]

$$\Lambda=\begin{cases}\sqrt{2} & \text{for bcc lattice}\\ \sqrt{3} & \text{for fcc lattice}\end{cases} \tag{9}$$

where a is the lattice parameter. ρ is the density of dislocation, which is assumed to depend on plastic strain [39]. A proposed form of ρ is [35,36].

$$\rho=\rho_0+\gamma\left(\bar{\varepsilon}_p\right)^{0.7} \tag{10}$$

where ρ_0 is the initial dislocation density of stress-free metal. γ is the coefficient of dislocation propagation. With Eqs. (1–10), equilibrium hydrogen concentration in a deformed metal can be calculated as function of elasto-plastic stress-strain response.

$$C=C_L+C_T=\beta\theta_L N_L+\alpha\theta_T N_T \qquad \text{H atom/m}^3$$

or

$$c=c_L+c_T=\frac{C_L}{N_L}+\frac{C_T}{N_L}=\beta\theta_L+\alpha\theta_T\frac{N_T}{N_L} \qquad \text{H atom/metal atom(H/M)} \tag{11}$$

Macroscopic plasticity model containing hydrogen induced lattice dilatation

In global scale, material is treated as continuum body. Hirth [40] stated that hydrogen dissolved in metal matrix induced isotropic expansion of the lattice, which is known as hydrogen induced dilatation. The strain of hydrogen influenced material is given by

$$\varepsilon_{ij}=\varepsilon_{ij}^e+\varepsilon_{ij}^h+\varepsilon_{ij}^p \tag{12}$$

where superscript e, p, h represent strain component of elastic deformation, plastic deformation and hydrogen induced dilatation respectively. Subscript i, j obey Einstein notation. Elastic component is given by

$$\varepsilon_{ij}^e=\frac{1+\nu}{E}\sigma_{ij}-\frac{\nu}{E}\sigma_{kk}\delta_{ij} \tag{13}$$

where E and ν are elastic module and Poisson's ratio in hydrogen free case. δ_{ij} is Kronecker function. Hydrogen induced dilatation is stated as [41].

$$\varepsilon_{ij}^h=\frac{1}{3}\frac{V_H}{V_M}(c-c_0)\delta_{ij} \tag{14}$$

Eq. (14) Indicates hydrogen induced lattice dilatation is isotropic and affects only spherical stress components of the material. Hydrogen's effect on yield stress depends on several factors such as hydrogen solubility, material microstructure, hydrogen source (internal or external) and loading rate [42]. For most commercial steels, severely stress-strain curve distort induced by hydrogen is not expected to happen [20,43–46]. Therefore, we assumed a hydrogen immune Mises yield criterion in global scale. This idea was also supported by existing HE models [35,47–49]. Plastic flow is defined by power law hardening and J2 flow law as

$$\begin{cases}\sigma_s=\sigma_0\left(1+\dfrac{\bar{\varepsilon}_p}{\varepsilon_0}\right)^n\\ f=\sqrt{\left(\dfrac{3}{2}s_{ij}s_{ij}\right)}-\sigma_s\\ \varepsilon_{ij}^p=\bar{\varepsilon}_p\dfrac{\partial f}{\partial\sigma_{ij}}\end{cases} \tag{15}$$

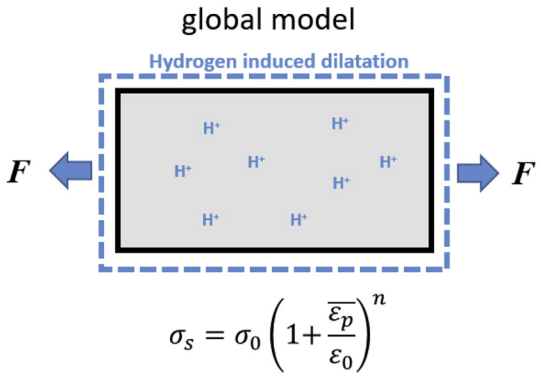

Fig. 1 – Global model for hydrogen damage material.

where σ_0 denotes initial yield stress. $\varepsilon_0 = \sigma_0/E$ is initial yielding strain. s_{ij} is the deviator components of stress. N is the index of power law hardening. $\overline{\varepsilon}_p$ is equivalent plastic strain. The global model is illustrated in Fig. 1. This model will provide far field stress & strain response for local damage evolution.

Mesoscopic ductile damage model involving HELP mechanism

For local matrix, hydrogen enhanced plasticity affects local mechanical behavior significantly. HELP mechanism is used to describe hydrogen's effect. Considering a continuum unit cell where ductile damage is expected to onset. HELP mechanism can be quantified with Sofronis et al. [21] model as

$$\sigma_f(c) = \sigma_s\varphi(c) = \sigma_0\varphi(c)\left(1+\frac{\overline{\varepsilon}_{pc}}{\varepsilon_{0c}}\right)^n \tag{16}$$

where $\overline{\varepsilon}_{pc}$ is local plastic strain enhanced by hydrogen. ε_{0c} is the local strain corresponds to initial yielding, $\varepsilon_{0c} = \sigma_0\Phi(c)/E$. $\Phi(c)$ is the influence function of hydrogen induced softening. Available $\Phi(c)$ forms can be found in the work of Liang et al. [23], Ahn et al. [25,26] and Falkenberg et al. [50]. All of them describes a liner function of absolute/relative hydrogen concentration or occupancy with a coefficient ξ. A proposed form of $\Phi(c)$ is [26].

$$\begin{cases} \varphi(c) = (\xi-1)\dfrac{c}{c_{L0}}+1 & \varphi(c) \geq \mu \\ \varphi(c) = \mu & \varphi(c) < \mu \end{cases} \tag{17}$$

where ξ is adjustable coefficient describing hydrogen susceptibility. μ denotes the lower boundary of hydrogen induced softening, which is used to avoid vanishing of local flow stress. $\mu = 0.1$ was used in the present work. c_{L0} is NILS hydrogen concentration in stress-free state equilibrating with 1 atm hydrogen pressure (0.1 MPa).

Similar with macroscopic response, local strain is stated as

$$\varepsilon_{ij}^{l} = \varepsilon_{ij}^{e,l} + \varepsilon_{ij}^{h,l} + \varepsilon_{ij}^{p,l} \tag{18}$$

where superscript l denotes the variables in local scale. In Eq. (18), elastic component and hydrogen dilatation component is inherited from macroscopic model with Eqs. (13) and (14). HELP influenced local plastic response is stated as

$$\begin{cases} \sigma_f(c) = \sigma_0\varphi(c)\left(1+\dfrac{\overline{\varepsilon}_{pc}}{\varepsilon_{0c}}\right)^n \\ f = \sqrt{\dfrac{3}{2}s_{ij}s_{ij}} - \sigma_f(c) \\ \varepsilon_{ij}^{p,l} = \overline{\varepsilon}_{pc}\dfrac{\partial f}{\partial\sigma_{ij}} \\ c(\sigma_m, \overline{\varepsilon}_{pc}) = \dfrac{(\alpha\theta_T N_T + \beta\theta_L N_L)}{N_L} \end{cases} \tag{19}$$

Ductile rupture is controlled by MVC process. In the view of continuum damage mechanics, ductile fracture is the result of damage accumulation. The cumulated damage is

$$\omega_f = \int_0^t d\omega \tag{20}$$

Fracture of a mass point occurs when accumulated damage ω_f becomes unity. According to the theory of Rice & Tracey [51], MVC induced fracture can be described by multi-axial fracture strain ε_f, which is proportional to stress triaxiality

$$\varepsilon_f \propto \exp\left(\frac{3\sigma_m}{2\sigma_f}\right) \tag{21}$$

In the works of Pfuff & Diezel [52], Kim et al. [35] and Jeon et al. [36], hydrogen reduced fracture strain was described as a linear function of NILS hydrogen concentration c_L. Ahn et al. [26] also indicated that HELP influenced local MVC depends on NILS hydrogen concentration c_L. In the present model, a suggested fracture strain is

$$\varepsilon_f(c_L) = A\exp\left(-1.5\frac{\sigma_m}{\sigma_f(c_L)}\right) + B \tag{22}$$

where A and B are the non-negative coefficients measured by experiment [53]. σ_f is local flow stress involved in hydrogen enhanced MVC process. Critical fracture condition is given as

$$\omega_f = \int_0^t \frac{d\overline{\varepsilon}_{pc}}{\varepsilon_f} = 1 \tag{23}$$

According to Eqs. (19) and (22), one can derive at any moment

$$\begin{matrix} \varepsilon_f(c) \leq \varepsilon_f(c=0) \\ d\overline{\varepsilon}_{pc}(c) \geq d\overline{\varepsilon}_p(c=0) \end{matrix} \tag{24}$$

which leads to

$$t(c) \leq t(c=0) \tag{25}$$

Eq. (25) Indicates reduced fracture strain and enhanced damage accumulation in the present of hydrogen, which have been experimentally observed [52,54]. The local model is shown in Fig. 2. According to Eq. (22), two synergistic effects on MVC damage evolution were described: (1) Enhanced

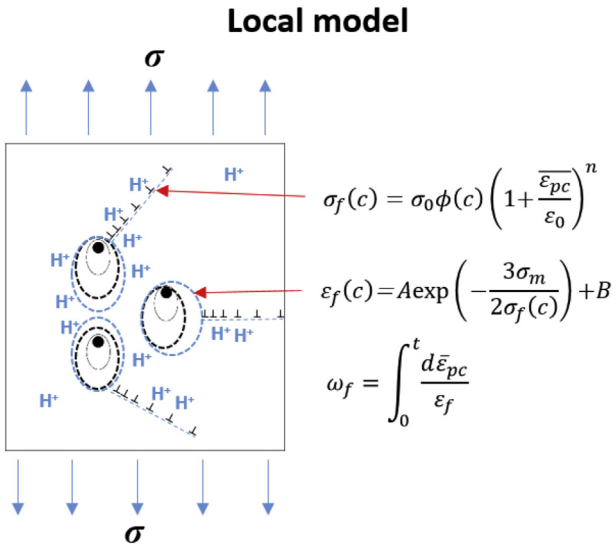

Fig. 2 – Local model for hydrogen damage material.

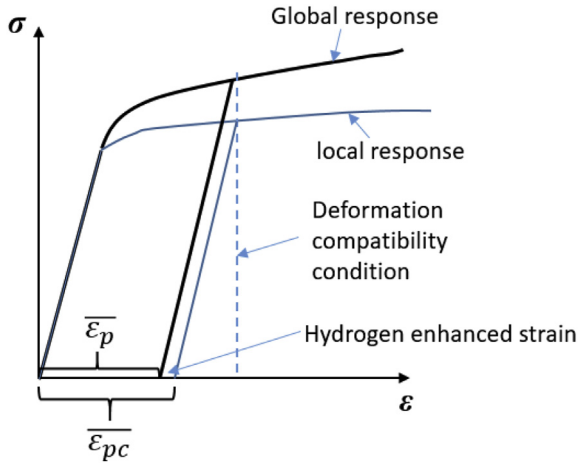

Fig. 3 – Deformation compatibility condition between global and local model.

localized plastic strain which promotes local hydrogen accumulation and further promoted plastic strain; (2) Softened flow stress which increase local stress triaxiality. These two effects represent HELP mechanism which lower fracture strain and enhance MVC damage accumulation.

Coupling of macro-to-mesoscopic HE model

The HE model is established based on coupling of above-mentioned global mechanical response model and local material damage model through deformation compatibility condition. The compatibility condition illustrated in Fig. 3 yields a nonlinear equation set

$$\begin{cases} \sigma_s = \sigma_0\left(1+\frac{\bar{\varepsilon}_p}{\varepsilon_0}\right)^n \\ \sigma_f = \sigma_0\varphi(c)\left(1+\frac{\bar{\varepsilon}_{pc}}{\varepsilon_{0c}}\right)^n \\ \bar{\varepsilon}_{pc} = \bar{\varepsilon}_p + \frac{\sigma_s-\sigma_f}{E} \\ c = c(\sigma_m,\ \bar{\varepsilon}_{pc}) \end{cases} \quad (26)$$

Eq. (26) uses the response of global model as far field stress and strain to evaluate local hydrogen enhanced plastic strain and hydrogen accumulation, which provides driven force of local hydrogen damage evolution.

Acting mechanism of the proposed damage model is summarized in Fig. 4. At global scale, a general elasto-plastic analysis provides stress & strain field which contains hydrogen induced lattice dilatation but without hydrogen induced damage. Through deformation compatibility condition, the driven force of far field stress & strain yields hydrogen enhanced localized plastic strain and hydrogen reduced fracture strain at local scale, which promotes damage accumulation and is considered as a representation of hydrogen-meditated MVC. Two synergistic effects acts: (1) Enhanced plastic strain as a result of hydrogen induced dislocation motion, which promotes local hydrogen redistribution and further plastic strain. (2) Reduced fracture strain induced by hydrogen promoted stress triaxiality. Synergistic action of these two effects accelerates MVC evolution (damage accumulation) in the present of hydrogen. Consequentially, fracture is triggered at lower global deformation, which is a phenomenon of HE.

Numerical examples and discussions

Model implementation

The proposed fracture strain model has been implemented on commercial software package ABAQUS with user subroutine VUHARD and VUSDFLD. The flowchart is shown in Fig. 5. The established model used explicit dynamic algorithm to overcome the nonlinear difficulty induced by local hydrogen damage and progressive damage evolution.

According to Sofronis [41], hydrogen induced lattice dilatation can be represented by using effective elastic module E_c and Poisson's ratio ν_c

$$\begin{aligned} E_c &= \frac{9EV_MRT}{9V_MRT + c_0V_H{}^2E} \\ \nu_c &= \frac{9\nu V_MRT - c_0V_H{}^2E}{9V_MRT + c_0V_H{}^2E} \end{aligned} \quad (27)$$

Notably, Eq. (27) shows how hydrogen induce lattice expansion. However, in common hydrogen systems constructed by iron and steel, hydrogen induced lattice expansion is relatively small due to small hydrogen solubility in structural steels. Therefore, hydrogen influence calculated by Eq. (27) Is usually neglectable. But still, hydrogen induced lattice dilatation is considered for accuracy purpose.

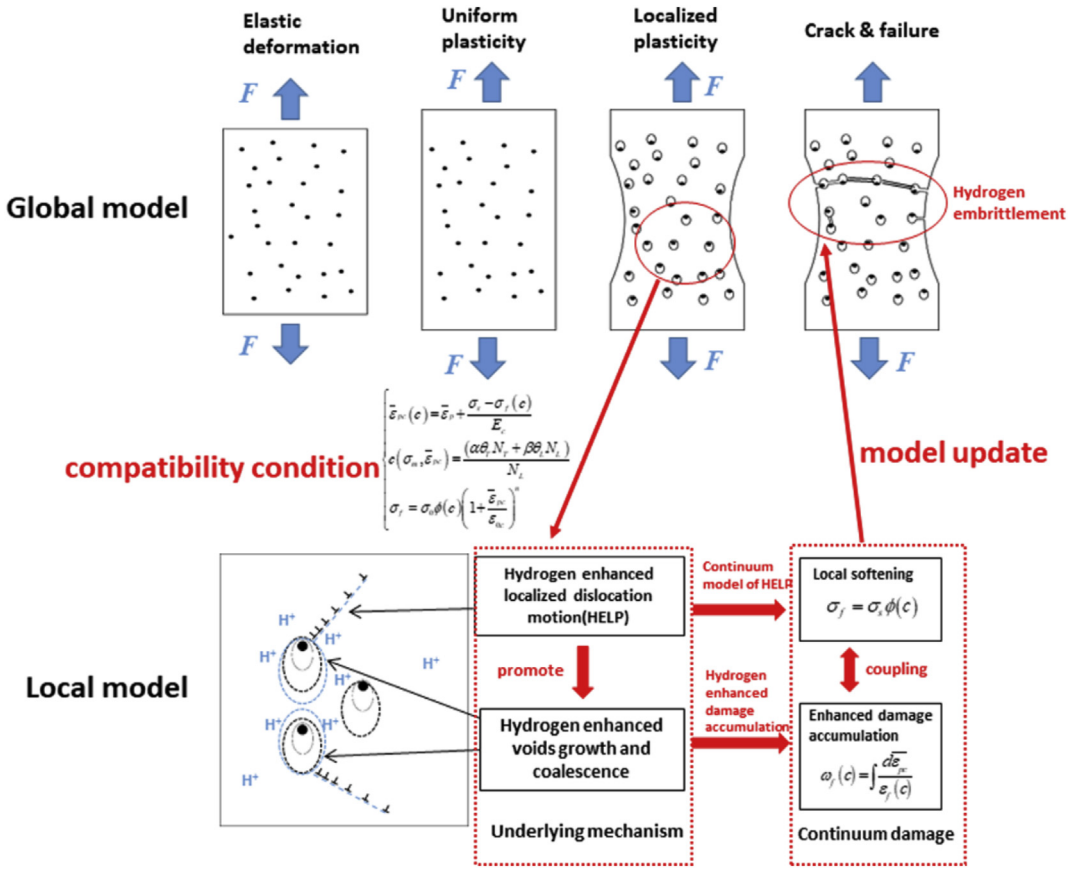

Fig. 4 – Acting mechanism of the proposed multi-scaled damage model.

Compact tensile test simulation of FeE 690T steel

Material properties

CT test of FeE 690T steel was investigated as an example of high constraint problem. This problem has been investigated by several works [27,35,50,55]. Hydrogen related parameters of FeE 690T are listed in Table 1. Material properties extracted from the stress-strain curves in Ref. [55] are listed in Table 2. Coefficients of FeE 690T fracture strain model was reported by Kim et al. [35] as

$$\varepsilon_f = 2.52\exp\left(-1.5\frac{\sigma_m}{\sigma_f(C_L)}\right) + 0.07 \tag{28}$$

Model setup

CT test were simulated in air and in hydrogen charged conditions. The investigated specimen is shown in Fig. 6(a). A 2D finite element model of 1/2 CT specimen was established with CPE4R plane strain element. The model contains 7100 elements and 7335 nodes. Mesh size around crack tip was refined as 0.02 mm. Constant velocity load was applied to the loading hole, as is shown in Fig. 6(b). Loading rate was 0.001 mm/s to keep the problem in quasi-static state. Environment hydrogen concentration was $C_{env} = 2.1 \times 10^{14}$ H atom/mm^3 [35]. $C_{L0} = C_{env}$ was considered for Eq. (17) As hydrogen charging was conducted in atmosphere. The results were compared with experimental result reported by Scheider et al. [55]. For all simulations, HELP parameter of $\xi = 0.8$ was used.

Simulation results

The simulated crack resistance curves (R-curves) are shown in Fig. 7, where δ_5 is the displacement measured at ±2.5 mm up and down the initial crack tip. According to Kim et al. [35], when loading rate is 0.001 mm/h (referred as CASE A), hydrogen diffusion can be considered as sufficient. Therefore, CASE A was numerically predicted with equilibrate hydrogen distribution described in Section Hydrogen concentration in equilibrate state. Loading speed 0.1 mm/h is a fast loading case (referred as CASE B) where hydrogen diffusion through lattice can be ignored. For CASE B, we used hydrogen distribution in Section Hydrogen concentration in equilibrate state but assumed constant NILS hydrogen concentration C_L=C_{env} to suppress influence of hydrogen diffusion. According to Fig. 7, the proposed method presents excellent consistency with experimental results in both hydrogen charged cases and hydrogen-free case (Air). The predicted results shows increasingly accelerated cracking process with increasing hydrogen concentration. A knockdown of cracking resistance has been identified for CASE A (dots in Fig. 7 denotes the results extracted with same time interval) while CASE B shows stable crack growth process. If we assume the parameter $\xi = 0.8$ is calibrated from one of CASE A/B, it can be concluded from the other CASE that the effect of different hydrogen concentration on crack growth has been predicted precisely.

Hydrogen distribution ahead of crack tip at $\delta_5 = 0.025$ mm is shown in Fig. 8. It depicts that for both CASE A/B, peak of

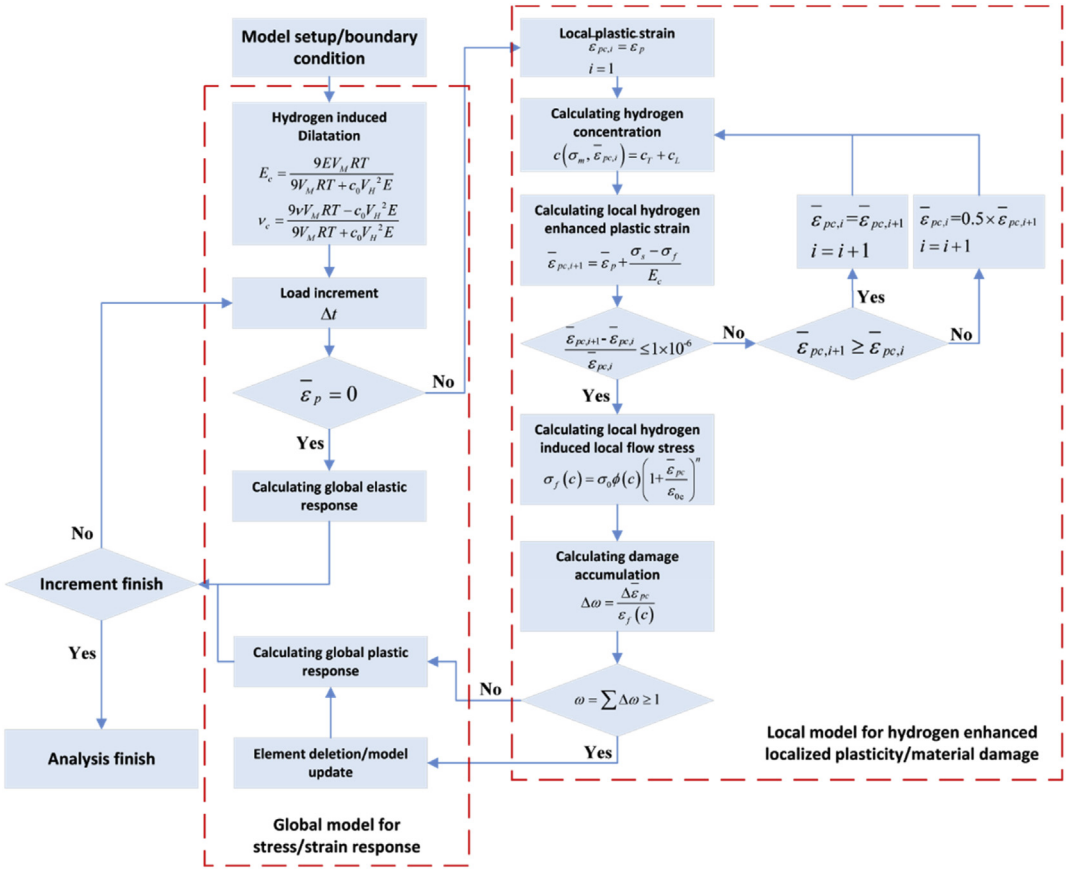

Fig. 5 – Flowchart of the proposed HE damage model.

Table 1 – Hydrogen related material properties of FeE 690T steel.

Parameter	Value	Note
Saturation hydrogen concentration C_{env}	3.7×10^{-10} mol/mm^3	Ref. [50,56]
Hydrogen bonding sites per trap α	1	
Number of NILS per metal atom β	6	
Dislocation density ρ_0	1.7859×10^{13} line length/m	
Dislocation density coefficient γ	9.7411×10^{14} line length/m	
Lattice parameter a	2.87×10^{-10} m	Ref. [38]
Trap binding energy W_B	42.1 kJ/mol	Ref. [35]
Molar volume of host metal V_M	7.12×10^{-6} m^3/mol	
Temperature T	298 K	

Table 2 – Mechanical properties of FeE 690T steel.

Parameter	Value	Note
Initial yield strength σ_0	693 MPa	Ref. [55]
Exponent of power law hardening n	0.087	
Young's modulus E	200 GPa	
Poisson's ratio ν	0.31	

hydrogen concentration C locates as crack tip and decreases sharply along crack depth direction. Due to stress induced hydrogen diffusion in CASE A, a peak of NILS hydrogen C_L is found at about 0.1 mm beneath crack tip with value about 4 times of C_{env}. C_L at crack surface is 2 times of C_{env}. For CASE B, C_L equals to C_{env} as hydrogen diffusion was suppressed. However, total hydrogen concentration C increase as a result of hydrogen diffusion (from CASE B to CASE A) is relatively small at crack tip but significant in the rest of bulk. This is attributed to high occupancy of trapped hydrogen. According to Oriani's theory [37], trapped hydrogen C_T is in equilibrate state with NILS hydrogen C_L, for trap binding energy of 42.1 kJ/mol, the occupancy of trap hydrogen is much higher than NILS hydrogen occupancy. Under this circumstances, the variation of C_L cannot lead to significant change of C at locations with pronounced dislocations accumulation (plastic zone). As a result, Fig. 8 demonstrated that at crack tip where MVC onsets, NILS hydrogen C_L of CASE A shows considerable difference with 2–4 times higher that of CASE B. But the difference between total hydrogen concentration of both cases is only about 1.2 times.

Hydrogen induced plastic strain($\bar{\varepsilon}_{pc} - \bar{\varepsilon}_p$) and hydrogen induced softening ($\sigma_s - \sigma_f$) along the crack tip are illustrated in Fig. 9. Cumulative damage distribution along crack tip is shown in Fig. 10. According to Fig. 9, hydrogen induced plasticity (enhanced strain and softened stress) is more significant in CASE A as hydrogen concentration at crack tip is higher in

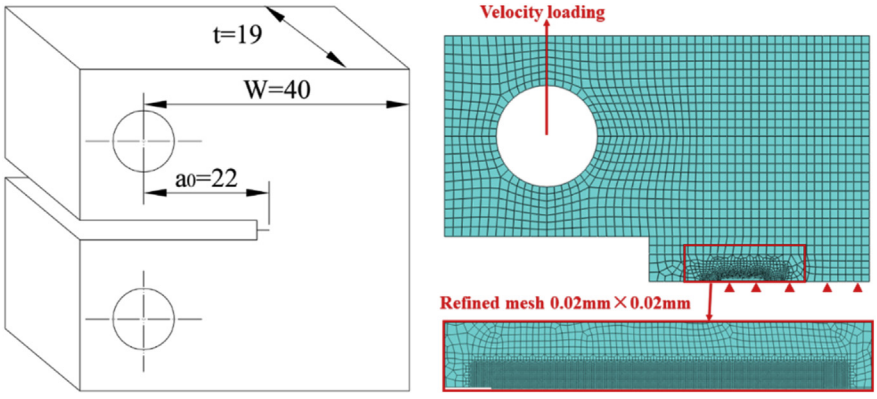

Fig. 6 – Illustration of CT specimen and model.

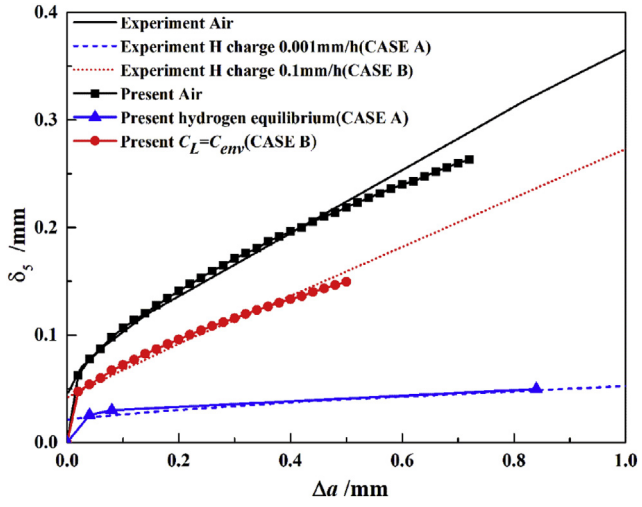

Fig. 7 – R-curves of CT specimen in hydrogen environment.

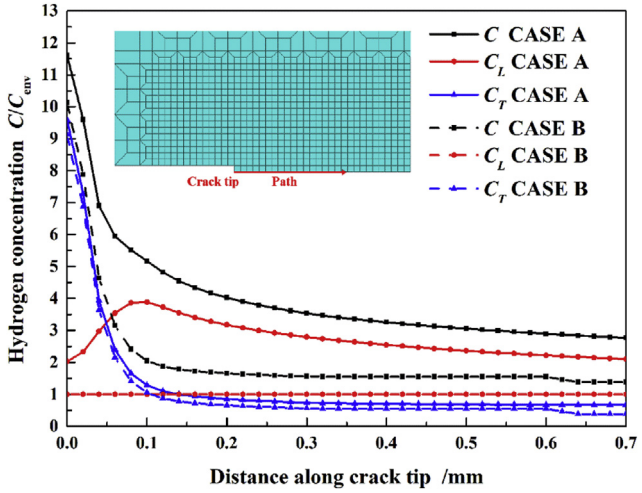

Fig. 8 – Hydrogen distribution along crack tip (δ_5 = 0.025 mm).

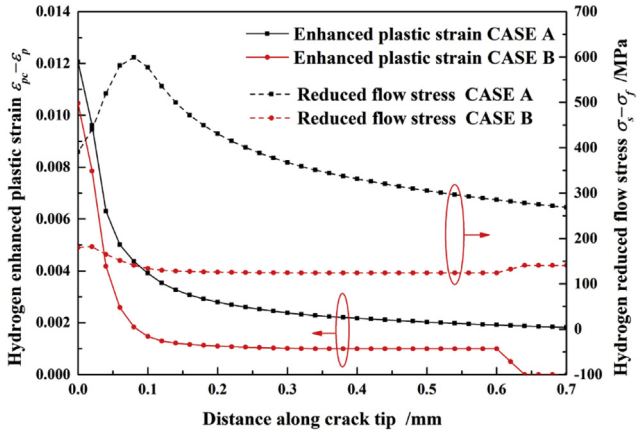

Fig. 9 – Hydrogen enhanced localized plasticity along crack tip (δ_5 = 0.025 mm).

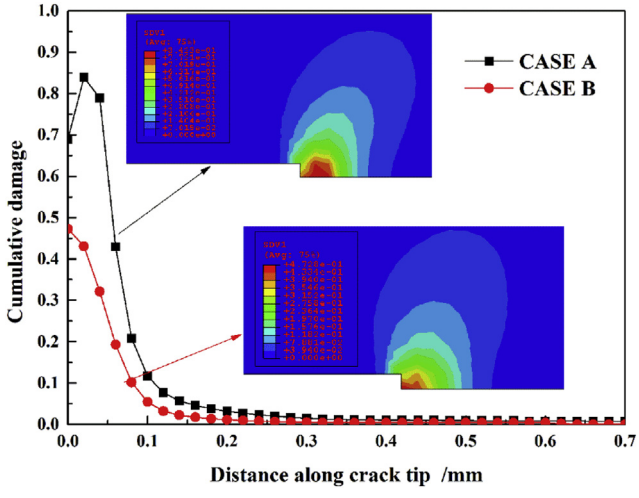

Fig. 10 – Cumulative damage distribution along crack tip (δ_5 = 0.025 mm).

this case. For Both CASE A & B, hydrogen enhanced local plastic strain reaches maximum at crack surface and decreases quickly along crack depth. The distribution of hydrogen enhanced plastic strain are similar with the distribution of total hydrogen concentration as shown in Fig. 9, which indicates that there is a positive feedback between hydrogen concentration C and enhanced plastic strain $\bar{\varepsilon}_{pc}$ as described by HELP mechanism. The present method determine $\bar{\varepsilon}_{pc}$ as a function of total hydrogen concentration C. Same idea has been adopted by many HELP related investigations [16,21,22,27,36,50,57]. Meanwhile, flow stress softening indicated by $(\sigma_s - \sigma_f)$ shows a similar distribution with NILS hydrogen concentration C_L. The dependency of fracture indications such as fracture strain and cohesive strength on hydrogen has been modeled as function of total hydrogen concentration [22,25,26], trapped hydrogen concentration [17,58] and NILS hydrogen concentration [27,35,36,50]. The present results supports the dependency of local fracture strain on NILS hydrogen concentration C_L, the idea is supported by Refs. [27,35,36,50,52]. According to Eqs. (22) and (23), both enhanced plastic strain and reduced flow stress contributes damage accumulation. Fig. 10 indicates that the damage accumulation ahead of crack tip in CASE A is faster than that in CASE B. Consequentially, crack grows faster in CASE A, which is considered as losing of crack growth resistance induced by HE.

Slow strain rate tensile test simulation of X80 steel

Material properties

SSRT test of X80 steel was investigated to illustrate the case without low constraints. SSRT experiments of X80 pipeline steel in different hydrogen pressures were reported by Refs. [59–61]. Based on the engineering stress-strain curve provided in Ref. [60]. Fracture strain model of X80 steel was calibrated as

$$\varepsilon_f = 3.6\exp\left(-1.5\frac{\sigma_m}{\sigma_f(c_L)}\right) + 0.05 \tag{29}$$

Mechanical properties and hydrogen related parameters of X80 steel were also collected from literatures. As listed in Table 3 and Table 4.

Table 3 – Hydrogen related material properties of X80 steel.

Parameter	Value	Note
Hydrogen bonding sites per trap α	10	Ref. [38,39]
Dislocation density ρ_0	1.72×10^{11} line length/m	
Dislocation density coefficient γ	4.06×10^{13} line length/m	
Lattice parameter a	2.87×10^{-10} m	
Number of NILS per metal atom β	1	
Trap binding energy W_B	50 kJ/mol	
Molar volume of host metal V_M	7.11×10^{-6} m^3/mol	
Hydrogen partial molar volume in metal V_H	2.0×10^{-6} m^3/mol	
Temperature T	300 K	
Solubility at 300 K	0.005434 molH_2/m^{3}MPa$^{0.5}$	

Table 4 – Mechanical properties of X80 steel.

Parameter	Value	Note
Initial yield strength σ_0	481 MPa	Ref. [59]
Exponent of power law hardening n	0.1176	
Young's modulus E	205 GPa	
Poisson's ratio ν	0.31	

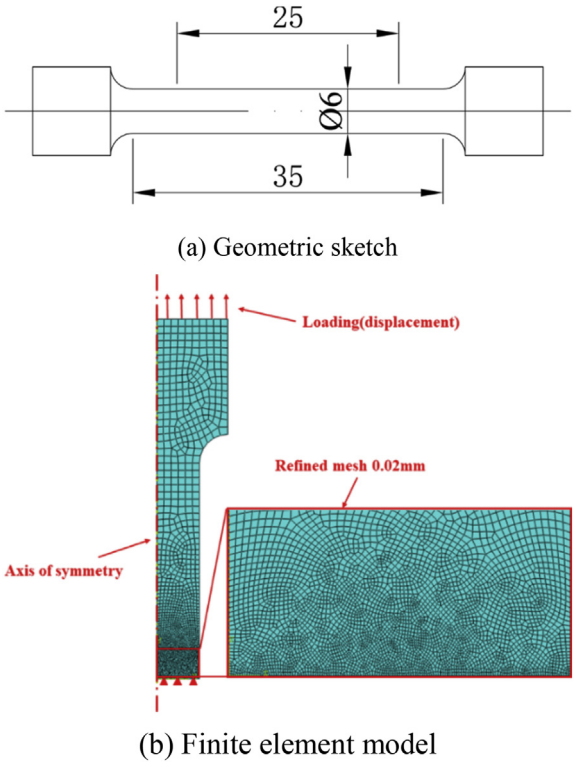

Fig. 11 – Illustration of SSRT specimen and model.

Model setup

The investigated specimen is a round bar with diameter of 6 mm and stroke length of 25 mm, as is shown in Fig. 11(a). 2D axisymmetric finite element model was established for 1/2 length of the specimen. Mesh size at interesting zone was refined to 0.02 mm for accuracy. The model has 4937 CAX4R elements and 5127 nodes. Symmetric boundary conditions was applied to bottom of the model, velocity boundary condition was applied on top of the model. Tensile strain rate was 6.7×10^{-5} s^{-1} to simulate quasi-static loading. The mesh and boundary conditions are illustrated in Fig. 11(b).

SSRT simulations were conducted in air and H_2 environment with different hydrogen pressure. Initial NILS hydrogen concentration c_L was determined by Sievert's law. For X80 steel, it is stated as [62].

$$c_L = 4.5 \times 10^{-8}\sqrt{p} \quad \text{H/M} \tag{30}$$

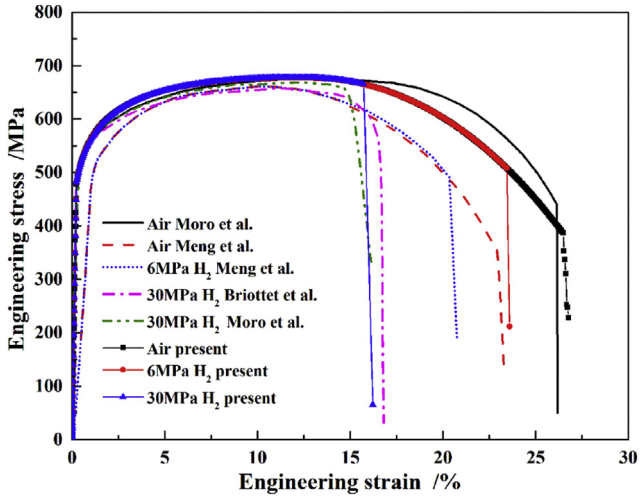

Fig. 12 – Engineering stress-strain curve of X80 steel.

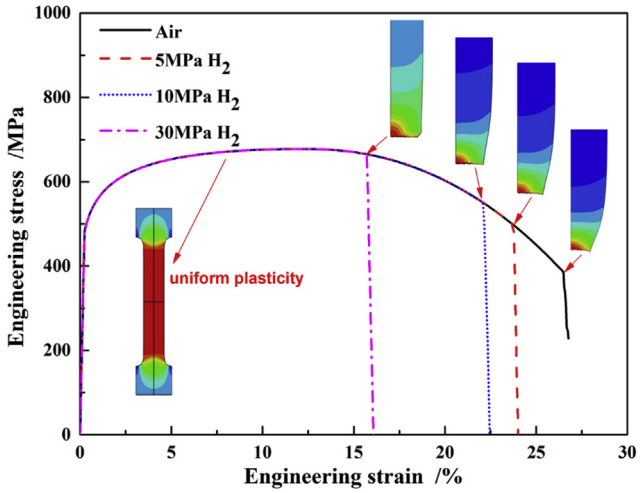

Fig. 13 – Stress-strain curves of X80 with different hydrogen pressure.

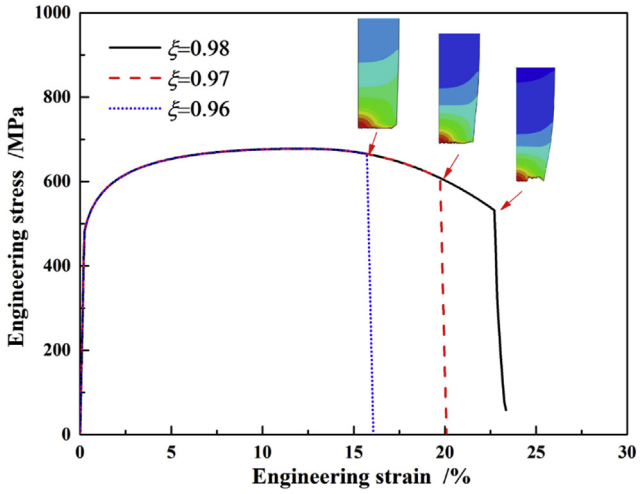

Fig. 14 – Stress-strain curves of X80 with different HELP parameter (30 MPa H_2).

where p is partial pressure of hydrogen measured in MPa. H/M denotes hydrogen atoms/per metal atom. c_{L0} required for Eq. (17) was calculated as 1.42×10^{-8} H/M with a 0.1 MPa H_2. HELP parameter $\xi = 0.96$ was used for all cases.

Simulation results

Predicted stress-strain curves of X80 steel in air, 6 MPa and 30 MPa H_2 are presented in Fig. 12. Experimental results from Moro et al. [59], Meng et al. [60] and Briottet et al. [61] are exhibited as well. It is shown that in the absent of hydrogen, stress-strain curve from the proposed method and experiments are coincided, which indicates that the proposed method predicted MVC dominated ductile fracture reasonably. When hydrogen is involved, it depicts a trend that decreasing tensile ductility with increasing hydrogen pressure. This phenomenon has been experimentally observed from hydrogen charged pipeline steels [44,59,60]. Define hydrogen susceptibility of SSRT test with reduction of elongation as

$$REL(\%) = \frac{E_l - E_{lc}}{E_l} \times 100\% \tag{31}$$

where E_l is elongation of SSRT specimen in air, E_{lc} is elongation in the present of hydrogen. *REL* of X80 steel under 6 MPa and 30 MPa H_2 are listed in Table 5. The data shows *REL* reproduced by the proposed method matches well with experimental results. Besides, these data also support the reasonability of HELP parameter $\xi = 0.96$ used for X80 steel. In summary, the present results are in good consistency with existing experimental observations, which verifies the rationality of the proposed method.

In order to illustrate the effect of Hydrogen pressure on HE of X80 steel. SSRT simulation was performed in 5 MPa, 10 MPa and 30 MPa H_2. Stress-strain curve of X80 steel in air, 5 MPa, 10 MPa and 30 MPa H_2 are shown in Fig. 13. It can be found both elongation and relative reduction of area (RRA) decrease simultaneously as hydrogen pressure increases. According to the profile of specimen shown in Fig. 13, necking effect is almost disappeared in 30 MPa H_2, indicating a very high susceptibility of X80 steel in 30 MPa H_2. Same conclusion has been obtained from experiments [61]. Another factor affecting the prediction is HELP parameter ξ which represents hydrogen susceptibility of material. In 30 MPa H_2, SSRT curves of X80 steel with different ξ is illustrated in Fig. 14. It can be found lower value of ξ represents higher hydrogen susceptibility, which produces more significant HE phenomenon.

Fig. 15 shows hydrogen concentration variation during straining at center of the specimen. Fig. 16 shows effect of HELP during straining at same location. As is shown in Fig. 15(a), total hydrogen concentrations variation induced by increasing hydrogen pressure is very limiting. When

Table 5 – Reduction of Elongation (*REL*) under different hydrogen pressure.

Hydrogen pressure	Experiment *REL*	Proposed method *REL*
6 MPa	11.0% [60]	12.0%
30 MPa	37.7% [61]	40.1%

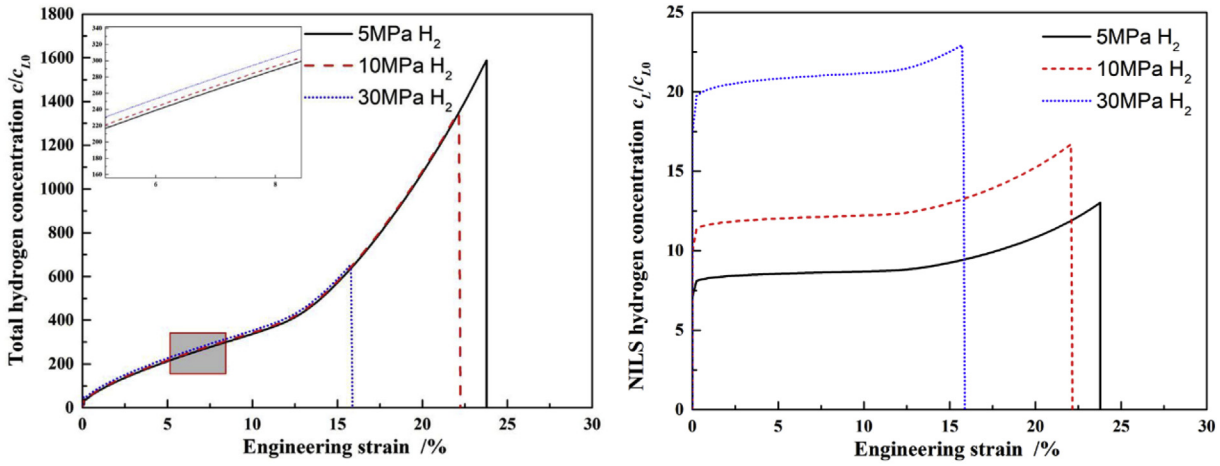

(a) Total hydrogen concentration (b) NILS hydrogen concentration

Fig. 15 – Hydrogen concentration at the center of SSRT specimen.

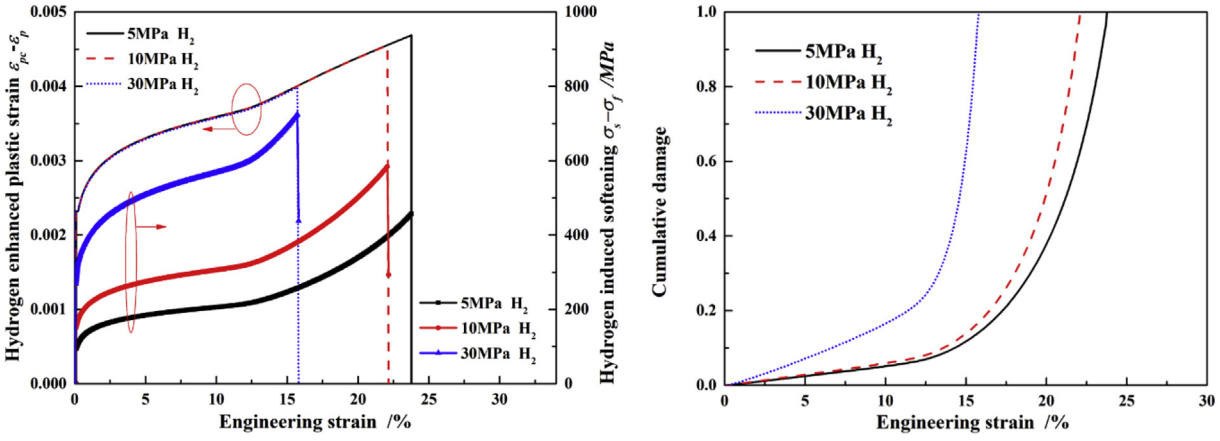

(a) HELP indications (a) Cumulative damage

Fig. 16 – Hydrogen enhanced damage evolution at center of SSRT specimen.

hydrogen pressure increased from 5 MPa to 30 MPa, total hydrogen concentration increases insignificantly (can be found in the zoom figure). As is mentioned, the reason is dominating amount of trapped hydrogen in plastic zone. As total hydrogen concentration is similar in different hydrogen pressures, the level of hydrogen enhanced plastic strain ($\bar{\varepsilon}_{pc} - \bar{\varepsilon}_p$) is similar in all cases, as is shown in Fig. 16(a). On the contrary, NILS hydrogen concentration in Fig. 15(b) depicts pronounced elevating as hydrogen pressure increases. Although Fig. 15 indicates NILS hydrogen concentration is about two magnitudes lower than trapped hydrogen concentration, NILS hydrogen can affect local damage evolution directly as it has been coupled into Eq. (22) In a way of hydrogen softened flow stress. As a result, MVC is accelerated by increasing local stress triaxiality induced by flow stress softening, which leads to faster damage accumulation in the case with higher hydrogen pressure. According to Fig. 16(b), damage accumulation accelerates after engineering strain is larger than about 12.5% which is necking strain according to Fig. 13. After necking, 30 MPa case exhibits the most steep damage climbs to critical damage ($\omega_c = 1$) with least deformation. It implies that stress localization induced by necking is a booster of damage accumulation, supporting the necessity of a stress concentration or high stress triaxiality to trigger HE. This trend coincides with the common sense that HE is onset from defects or micro-crack in the structure [12,13,15,18,63].

Discussions

Hydrogen concentration introduced by pressurized environment or cathodic charging is a primary factor affecting the level of HE. Both the results of CT simulation and SSRT

simulation indicated the proposed method has reproduced a trend of increasing HE susceptibility as hydrogen contents increases. This susceptibility is represented by increasingly reduced crack growth resistance of CT specimen and losing of elongation and RRA of SSRT specimen with elevating of hydrogen contents, which agrees with extensive experimental observations [64]. Another inherent factor is hydrogen compatibility of material representing by HELP parameter ξ. According to the definition of ξ, it represents the level of strength softening when material is immersed into 1 atm hydrogen pressure and the diffusion has been sufficient. Therefore, lower ξ value implies less compatible with hydrogen. As is shown in the simulations, FeE 690T steel (this steel is similar with X100 steel in compositions and mechanical properties [55]) is more susceptible with hydrogen than X80. This conclusion is supported by experiments [65]. Therefore it can be concluded that the proposed method has reproduced hydrogen's effect on material properties reasonably. Noteworthy, due to the small solubility of hydrogen in bcc steels, the present examples did not exhibited noticeable influence of hydrogen induced lattice dilatation, which was considered as hydrogen influenced elastic module and Poisson's ratio [41]. It is expected to be more pronounced in system with higher hydrogen solubility such as fcc steel or Niobium [22].

In the present work, HE phenomenon was investigated on two typical configurations with different constraints (CT and SSRT). Ductile fracture (cup-cone fracture of SSRT test) was reproduced for both problems in the absent of hydrogen. In the present of hydrogen, fast crack growth (CT test) and ductility loss (SSRT test) were predicted. The results indicates ductile damage based HE model using HELP mechanism, i.e. HELP based MVC fracture could be a viable model for the prediction of HE. Ahn et al. [26] investigated interaction between hydrogen and micro-voids in A533B steel with HELP mechanism, the results suggests that hydrogen can promote both void growth and coalescence. At low stress triaxiality, this promotion is primarily controlled by hydrogen enhanced shear localization between voids [22,25]. At high stress triaxiality, hydrogen's effect is more pronounced as it influences both growth rate and critical strain of coalescence. In the proposed method, Eq. (22) describes a fracture strain lowered by NILS hydrogen. The underlying of hydrogen reduced fracture strain is hydrogen enhanced void coalescence. This term is also known as hydrogen-assisted "internal necking" and shear localization, which is effective in interpreting some hydrogen induced experimental phenomenon [22–25,66,67]. Eq. (23) Introduces HELP's effect into the accumulating process of ductile damage, which represents hydrogen promotes void growth in continuum sense. With the synergistic action of both Eqs. (22) and (23), hydrogen can promote ductile damage evolution greatly to trigger phenomenal "brittle" fracture.

Technically, it is preferable that a presumed HE model contains model parameters as less as possible because hydrogen related model calibration is usually expensive and inefficient. In this sense, the proposed method is very practical as it contains only one parameter ξ which can be calibrated with one SSRT or CT test in hydrogen environment easily. This advantage is achieved through the coupled description of HELP induced deformation behavior, i.e. enhanced localized plastic strain and HELP influenced MVC evolution into continuum damage model framework. As a result, quantify of HE with a single hydrogen related model (Eq. (17)) is possible.

Conclusions

In this work, a continuum damage model coupled with HELP mechanism was proposed for quantifying HE phenomenon of structural steel. The model coupled HELP mechanism into both MVC growth and coalescence, which describes a hydrogen accelerated ductile damage evolution process. The proposed model was performed numerically with ABAQUS user subroutine VUHARD and VUSDFLD. CT test and SSRT test were investigated numerically for validation purpose. Following conclusions can be draw:

(1) The proposed model reproduced experimental results of CT test and SSRT test under different hydrogen contents cases reasonably.
(2) The proposed model supports the feasibility of describing HE with ductile damage based methods. Phenomenal "embrittlement" of hydrogen related fracture can be rationalized by HELP mechanism through the synergistic action of hydrogen enhanced localized plasticity and hydrogen enhanced micro-voids growth & coalescence.
(3) Ductile fracture of structural steel and its detrimental transition induced by HE has been coupled into one continuum damage model. The proposed model is also highlighted with the advantage of practical as there is few model parameters.

Declaration of competing interest

The authors declare that they have no known competing financial interests or personal relationships that could have appeared to influence the work reported in this paper.

Acknowledgement

This work was supported by the National Natural Science Foundation of China- Natural Science Foundation for youth scientist(Grand No. 51905173).

REFERENCES

[1] Zheng J, Liu X, Xu P, Liu P, Zhao Y, Yang J. Development of high pressure gaseous hydrogen storage technologies. Int J Hydrogen Energ 2012;37:1048–57.
[2] Dwivedi SK, Vishwakarma M. Hydrogen embrittlement in different materials: a review. Int J Hydrogen Energ 2018;43:21603–16.

[3] Stan L. Discussion of some recent literature on hydrogen-embrittlement mechanisms: addressing common misunderstandings. Corros Rev 2019;37:377–95.
[4] Troiano AR. The role of hydrogen and other interstitials in the mechanical behavior of metals. Metallog Microstruct Analysis 2016;5:557–69.
[5] Oriani RA, Josephic PH. Equilibrium aspects of hydrogen-induced cracking of steels. Acta Metall 1974;22:1065–74.
[6] Nagumo M. Mechanistic aspects of fracture I~ brittle fracture models, fundamentals of hydrogen embrittlement. Springer; 2016. p. 197–215.
[7] Nagao A, Smith CD, Dadfarnia M, Sofronis P, Robertson IM. The role of hydrogen in hydrogen embrittlement fracture of lath martensitic steel. Acta Mater 2012;60:5182–9.
[8] Dong CF, Liu ZY, Li XG, Cheng YF. Effects of hydrogen-charging on the susceptibility of X100 pipeline steel to hydrogen-induced cracking. Int J Hydrogen Energ 2009;34:9879–84.
[9] Koyama M, Tasan CC, Akiyama E, Tsuzaki K, Raabe D. Hydrogen-assisted decohesion and localized plasticity in dual-phase steel. Acta Mater 2014;70:174–87.
[10] Birnbaum HK, Sofronis P. Hydrogen-enhanced localized plasticity—a mechanism for hydrogen-related fracture. Mater Sci Eng 1994;176:191–202.
[11] Nagumo M. Mechanistic aspects of fracture II~ plasticity-dominated fracture models, fundamentals of hydrogen embrittlement. Springer; 2016. p. 217–39.
[12] Robertson IM, Sofronis P, Nagao A, Martin ML, Wang S, Gross DW, et al. Hydrogen embrittlement understood. Metall Mater Trans 2015;46:2323–41.
[13] Dadfarnia M, Nagao A, Wang S, Martin ML, Somerday BP, Sofronis P. Recent advances on hydrogen embrittlement of structural materials. Int J Fracture 2015;196:223–43.
[14] Martin ML, Dadfarnia M, Nagao A, Wang S, Sofronis P. Enumeration of the hydrogen-enhanced localized plasticity mechanism for hydrogen embrittlement in structural materials. Acta Mater 2019;165:734–50.
[15] Djukic MB, Bakic GM, Sijacki Zeravcic V, Sedmak A, Rajicic B. The synergistic action and interplay of hydrogen embrittlement mechanisms in steels and iron: localized plasticity and decohesion. Eng Fract Mech 2019;216:106528.
[16] Barrera O, Tarleton E, Tang HW, Cocks ACF. Modelling the coupling between hydrogen diffusion and the mechanical behaviour of metals. Comp Mater Sci 2016;122:219–28.
[17] Novak P, Yuan R, Somerday BP, Sofronis P, Ritchie RO. A statistical, physical-based, micro-mechanical model of hydrogen-induced intergranular fracture in steel. J Mech Phys Solids 2010;58:206–26.
[18] Birnbaum HK. Hydrogen effects on deformation and fracture: science and sociology. MRS Bull 2003;28:479–85.
[19] Gerberich WW, Stauffer DD, Sofronis P. A coexistent view of hydrogen effects on mechanical behavior of crystals: HELP and HEDE. In: Somerday B SPJR, editor. 2008 International hydrogen conference-effects of hydrogen on materials. Wyoming, USA. Ohio: ASM International, Jackons Lake Lodge, Grand Teton National Park; 2009. p. 38–45.
[20] Yu H, Olsen JS, Alvaro A, Qiao L, He J, Zhang Z. Hydrogen informed Gurson model for hydrogen embrittlement simulation. Eng Fract Mech 2019;217:106542.
[21] Sofronis P, Liang Y, Aravas N. Hydrogen induced shear localization of the plastic flow in metals and alloys. Eur J Mech Solid 2001;20:857–72.
[22] Liang Y, Ahn DC, Sofronis P, Dodds RH, Bammann D. Effect of hydrogen trapping on void growth and coalescence in metals and alloys. Mech Mater 2008;40:115–32.
[23] Liang Y, Sofronis P, Dodds RH. Interaction of hydrogen with crack-tip plasticity: effects of constraint on void growth. Mater Sci Eng 2004;366:397–411.
[24] Liang Y, Sofronis P, Aravas N. On the effect of hydrogen on plastic instabilities in metals. Acta Mater 2003;51:2717–30.
[25] Ahn DC, Sofronis P, Dodds RH. On hydrogen-induced plastic flow localization during void growth and coalescence. Int J Hydrogen Energ 2007;32:3734–42.
[26] Ahn DC, Sofronis P, Dodds R. Modeling of hydrogen-assisted ductile crack propagation in metals and alloys. Int J Fracture 2007;145:135–57.
[27] Brocks W, Falkenberg R, Scheider I. Coupling aspects in the simulation of hydrogen-induced stress-corrosion cracking. Procedia IUTAM 2012;3:11–24.
[28] Jemblie L, Olden V, Akselsen OM. A review of cohesive zone modelling as an approach for numerically assessing hydrogen embrittlement of steel structures. Philos Trans A Math Phys Eng Sci 2017;375.
[29] Asadipoor M, Kadkhodapour J, Pourkamali Anaraki A, Sharifi SMH, Darabi AC, Barnoush A. Experimental and numerical investigation of hydrogen embrittlement effect on microdamage evolution of advanced high-strength dual-phase steel. Met Mater Int 2020. https://doi.org/10.1007/s12540-020-00681-1. In press.
[30] Olden V, Thaulow C, Johnsen R, Østby E. Cohesive zone modeling of hydrogen-induced stress cracking in 25% Cr duplex stainless steel. Scripta Mater 2007;57:615–8.
[31] Barrows W, Dingreville R, Spearot D. Traction–separation relationships for hydrogen induced grain boundary embrittlement in nickel via molecular dynamics simulations. Mater Sci Eng 2016;650:354–64.
[32] Jemblie L, Olden V, Mainçon P, Akselsen OM. Cohesive zone modelling of hydrogen induced cracking on the interface of clad steel pipes. Int J Hydrogen Energ 2017;42:28622–34.
[33] Alvaro A, Olden V, Akselsen OM. 3D cohesive modelling of hydrogen embrittlement in the heat affected zone of an X70 pipeline steel – Part II. Int J Hydrogen Energ 2014;39:3528–41.
[34] Serebrinsky S. A quantum-mechanically informed continuum model of hydrogen embrittlement. J Mech Phys Solids 2004;52:2403–30.
[35] Kim N, Oh C, Kim Y, Yoon K, Ma Y. Hydrogen-assisted stress corrosion cracking simulation using the stress-modified fracture strain model. J Mech Sci Technol 2012;26:2631–8.
[36] Jeon J, Larrosa NO, Oh Y, Kim Y, Ainsworth RA. Characterization of the effect of notch bluntness on hydrogen embrittlement and fracture behavior using FE analyses. In: ASME 2015 pressure vessels and piping Conference; 2015.
[37] Oriani RA. The diffusion and trapping of hydrogen in steel. Acta Metall 1970;18:147–57.
[38] Dadfarnia M, Martin ML, Nagao A, Sofronis P, Robertson IM. Modeling hydrogen transport by dislocations. J Mech Phys Solids 2015;78:511–25.
[39] Kumnick AJ, Johnson HH. Deep trapping states for hydrogen in deformed iron. Acta Metall 1980;28:33–9.
[40] Hirth JP. Effects of hydrogen on the properties of iron and steel. Metallurgical Transactions A 1980;11:861–90.
[41] Sofronis P. The influence of mobility of dissolved hydrogen on the elastic response of a metal. J Mech Phys Solids 1995;43:1385–407.
[42] Nagumo M. Deformation behaviors. In: Nagumo M, editor. Fundamentals of hydrogen embrittlement. Singapore: Springer Singapore; 2016. p. 79–101.
[43] Hua Z, Zhang X, Zheng J, Gu C, Cui T, Zhao Y, et al. Hydrogen-enhanced fatigue life analysis of Cr–Mo steel high-pressure vessels. Int J Hydrogen Energ 2017;42:12005–14.
[44] Nanninga NE, Levy YS, Drexler ES, Condon RT, Stevenson AE, Slifka AJ. Comparison of hydrogen embrittlement in three pipeline steels in high pressure gaseous hydrogen environments. CORROS SCI 2012;59:1–9.

[45] Baek UB, Lee HM, Baek SW, Nahm SH. Hydrogen embrittlement for X-70 pipeline steel in high pressure hydrogen gas. In: ASME 2015 pressure vessels and piping conference. American Society of Mechanical Engineers Digital Collection; 2015.
[46] Matsunaga H, Yoshikawa M, Kondo R, Yamabe J, Matsuoka S. Slow strain rate tensile and fatigue properties of Cr–Mo and carbon steels in a 115 MPa hydrogen gas atmosphere. Int J Hydrogen Energ 2015;40:5739–48.
[47] Gobbi G, Colombo C, Miccoli S, Vergani L. A weakly coupled implementation of hydrogen embrittlement in FE analysis. Finite Elem Anal Des 2018;141:17–25.
[48] Del Busto S, Betegón C, Martínez-Pañeda E. A cohesive zone framework for environmentally assisted fatigue. Eng Fract Mech 2017;185:210–26.
[49] Wang Y, Gong J, Jiang W. A quantitative description on fracture toughness of steels in hydrogen gas. Int J Hydrogen Energ 2013;38:12503–8.
[50] Falkenberg R, Brocks W, Dietzel W, Scheider I. Modelling the effect of hydrogen on ductile tearing resistance of steels. Int J Mater Res 2010;101:989–96.
[51] Rice JR, Tracey DM. On the ductile enlargement of voids in triaxial stress fields*. J Mech Phys Solids 1969;17:201–17.
[52] Pfuff M, Dietzel W. Mesoscale modelling of hydrogen assisted crack growth in heterogeneous materials. In: Carpinteri A, editor. Proc of the 11th Int Conf on Fracture. Italy: Turin; 2005.
[53] Oh C, Kim N, Kim Y, Baek J, Kim Y, Kim W. A finite element ductile failure simulation method using stress-modified fracture strain model. Eng Fract Mech 2011;78:124–37.
[54] Dietzel W, Pfuff M, Juilfs GG. Hydrogen permeation in plastically deformed steel membranes. Mater Sci+ 2006;42:78–84.
[55] Scheider I, Pfuff M, Dietzel W. Simulation of hydrogen assisted stress corrosion cracking using the cohesive model. Eng Fract Mech 2008;75:4283–91.
[56] Dietzel W, Pfuff M, Juilfs GG. Hydrogen permeation in plastically deformed steel membranes. MATER SCI+ 2006;42:78–84.
[57] Cui TC, Liu PF, Gu CH. Finite element analysis of hydrogen diffusion/plasticity coupled behaviors of low-alloy ferritic steel at large strain. Int J Hydrogen Energ 2017;42:20324–35.
[58] Liang Y, Sofronis P. Toward a phenomenological description of hydrogen-induced decohesion at particle/matrix interfaces. J Mech Phys Solids 2003;51:1509–31.
[59] Moro I, Briottet L, Lemoine P, Andrieu E, Blanc C, Odemer G. Hydrogen embrittlement susceptibility of a high strength steel X80. Mater Sci Eng 2010;527:7252–60.
[60] Meng B, Gu C, Zhang L, Zhou C, Li X, Zhao Y, et al. Hydrogen effects on X80 pipeline steel in high-pressure natural gas/hydrogen mixtures. Int J Hydrogen Energ 2017;42:7404–12.
[61] Briottet L, Batisse R, de Dinechin G, Langlois P, Thiers L. Recommendations on X80 steel for the design of hydrogen gas transmission pipelines. Int J Hydrogen Energ 2012;37:9423–30.
[62] Mine Y, Kimoto T. Hydrogen uptake in austenitic stainless steels by exposure to gaseous hydrogen and its effect on tensile deformation. Corros Sci 2011;53:2619–29.
[63] Djukic MB, Bakic GM, Zeravcic VS, Sedmak A, Rajicic B. Hydrogen embrittlement of industrial components: prediction, prevention, and models. Corros-US 2016;72:943–61.
[64] Marchi CS, Somerday BP. Technical reference for hydrogen compatibility of materials. 2012.
[65] Zhang T, Zhao W, Li T, Zhao Y, Deng Q, Wang Y, et al. Comparison of hydrogen embrittlement susceptibility of three cathodic protected subsea pipeline steels from a point of view of hydrogen permeation. Corros Sci 2018;131:104–15.
[66] Cialone H, Asaro RJ. The role of hydrogen in the ductile fracture of plain carbon steels. Metallurg Transac A 1979;10:367–75.
[67] Garber R, Bernstein IM, Thompson AW. Hydrogen assisted ductile fracture of spheroidized carbon steels. Metallurg Transac A 1981;12:225–34.